DOI: 10.1002/adma.200601867

Observation of van der Waals Driven Self-Assembly of MoSI Nanowires into a Low-Symmetry Structure Using Aberration-Corrected Electron Microscopy**

By *Valeria Nicolosi*, *Peter D. Nellist*,* *Stefano Sanvito*,* *Eireann C. Cosgriff*, *Satheesh Krishnamurthy*, *Werner J. Blau*, *Malcolm L. H. Green*, *Damjan Vengust*, *Damjan Dvorsek*, *Dragan Mihailovic*, *Giuseppe Compagnini*, *Jeremy Sloan*, *Vlad Stolojan*, *J. David Carey*, *Stephen J. Pennycook*, and *Jonathan N. Coleman**

One-dimensional nanowires have the potential to influence technology in areas from nanoscale logic elements[1] to advanced sensors[2] in a way that will radically change the world in which we live. Although the most common one-dimensional nanostructure is the carbon nanotube, attention is moving to structures such as MoS_2–$I_{1/3}$ nanotubes.[3] Recently, a new form of metal–chalcogenide–halide nanowire with the stoichiometry $Mo_6S_{9-x}I_x$ has been reported.[4] This material can be fabricated in a single-step process and consists of sub-nanometer-diameter nanowires that self-assemble into weakly bound bundles. These wires are conductive[5] and all have identical electronic properties.[6] In addition, they can easily be dispersed in common solvents[7,8] down to individual nanowires.[5,9] These materials have already displayed promise as field-emission tips[10] and in nanotribological applications.[11]

However, realization of the vast potential of these structures has been hampered by a lack of insight into their structure. A number of studies based on X-ray diffraction (XRD) have resulted in only moderate success.[6,12] Although this is partly caused by low sample purity, XRD studies on nanoscale systems are generally problematic because of the presence of diffuse components caused by the lack of long range order. To overcome this problem, both extended X-ray-absorption fine-structure[6] (EXAFS) and XRD measurements incorporating atomic pair-distribution-function[12] (PDF) analysis have been carried out to determine the average local structure. However, although these techniques could successfully identify the overall atomic skeleton of an individual nanowire, neither technique can detect subtle differences in the occupancy of the S and I atom sites, nor correctly determine the nanowire-bundle crystal superstructure. Both of these factors are crucial: the peripheral sites where either S or I reside control the interaction of the wire with other wires and with its external environment. Thus, to fully understand the structure of these novel compounds, an entirely new approach is required.

In this work we have used both high-resolution transmission electron microscopy (HRTEM) and, in particular, annular dark-field (ADF) imaging using an aberration-corrected scanning TEM (STEM) to examine low-diameter bundles of $Mo_6S_3I_6$ nanowires. The recent development of aberration correction in TEM and STEM has revolutionized the performance of these microscopes.[13–15] After correction, even a relatively low (100 kV) accelerating voltage allows us to attain a spatial resolution close to 0.1 nm, allowing unambiguous atomic-resolution imaging of the nanowires, while limiting their damage under electron radiation. ADF STEM is a powerful technique that provides direct atomic imaging of structures with image intensities depending strongly on atomic number, Z.[16] Detailed image analysis and simulation allowed us to ascertain, not only the locations of the atomic species in the unit cell of the individual wires, but also the supercell of the bundle. X-ray photoelectron spectroscopy (XPS) measurements confirmed our findings. Knowledge of

[*] Dr. P. D Nellist,[+] Prof. S. Sanvito, Dr. J. N. Coleman, Dr. V. Nicolosi, E. C. Cosgriff,[+] Dr. S. Krishnamurthy, Prof. W. J. Blau
School of Physics, Trinity College Dublin, University of Dublin
Dublin 2 (Ireland)
E-mail: peter.nellist@materials.ox.ac.uk; sanvitos@tcd.ie; colemaj@tcd.ie

Prof. S. J. Pennycook
Condensed Matter Division, Oak Ridge National Laboratory
Oak Ridge, TN 37831 (USA)

Prof. M. L. H. Green
Inorganic Chemistry Lab, University of Oxford
S Parks Road, Oxford, OX1 3QR (UK)

D. Vengust, Dr. D. Dvorsek, Prof. D. Mihailovic
Jozef Stefan Institute
Ljubljana, 1000 (Slovenia)

Prof. G. Compagnini
Department of Chemistry, University Catania
Viale A. Doria 6, Catania, 95125 (Italy)

Dr. J. Sloan, Dr. V. Stolojan, Dr. J. D. Carey
Advanced Technology Institute, University of Surrey
Guildford, GU2 7XH (UK)

[+] Present address: University of Oxford, Dept. of Materials, Parks Road, Oxford, OX1 3PH, UK.

[**] The authors acknowledge the support of the European Union in the form of the European Community's Human Potential Program under contract HPRN-CT-2002-00192, [NANOTEMP]. S.S. thanks the Science Foundation of Ireland (SFI02/IN1/I175) for financial support. D.M. and W.J.B. thank DESYGN-IT for financial support. We also thank the UK SuperSTEM facility for use of their facilities. V.N. and G.C. acknowledge A. Scandurra for useful discussions. Supporting Information is available online from Wiley InterScience or from the author.

© 2007 WILEY-VCH Verlag GmbH & Co. KGaA, Weinheim

ADVANCED MATERIALS

the crystalline structure allowed us to calculate the electronic structure, confirming the material's metallicity and the nature of the chemical bonds.

As-produced $Mo_6S_3I_6$ material has a wool-like appearance, with strands of 50–300 nm in diameter and up to 5 mm in length, as shown in Figure 1A. However, on sonication in suitable solvents,[7] the strands disperse into low-diameter[9] bundles similar to that shown in Figure 1B. At the concentration used for sample preparation, the bundle diameter varied between 1 and 40 nm, as measured by atomic force microscopy (Supporting Information, Fig. S1A and B). However, there was always a population of objects with diameter of approximately 1 nm (Supporting Information, Fig. S1B): we identify these as individual nanowires. They were also observed in STEM images, but were found to quickly damage under electron irradiation, unlike larger bundles, which showed greater stability.

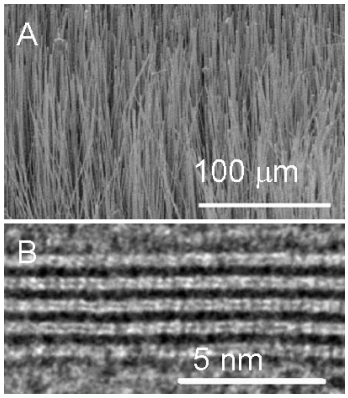

Figure 1. A) An SEM image of as-produced $Mo_6S_3I_6$ nanowire material. B) A HRTEM image showing a bundle of individual $Mo_6S_3I_6$ nanowires.

Previous authors have used XRD[6] and EXAFS[12] analysis to determine the $Mo_6S_3I_6$ nanowire structure. In both cases a structure similar to that shown in Figure 2A was presented. In this figure the red spheres represent Mo atoms, whose positions could accurately be determined by XRD. The purple and yellow spheres depict two distinct types of atomic site, which we will call peripheral (P) and linkage (L) sites, respectively. These studies could accurately determine the positions of both P and L sites but could not determine their occupancy in terms of S or I atoms other than to suggest that the L sites were occupied by I atoms. Shown in Figure 2B is the end-on view of the nanowire shown in Figure 2A. Also shown are the atomic planes containing both Mo atoms and P sites, which we call mixed planes (Planes 1 and 2). For comparison, an end view of the plane containing the L sites, the L plane, is also shown (Plane 3). In this scheme the atoms in the P sites are S or I depending on the stoichiometry. It is then suggested that these strands close-pack into bundles. Space groups of hexagonal-lattice $P6_3$ (#173)[3] and trigonal lattice $R\bar{3}$ (#148)[6,17,18] have previously been used to describe the packing. Shown in Figure 3A is a HRTEM image showing the cross section of a bundle. This image confirms the near-hexagonal close-packing of the wires in the bundle with a center-to-center distance of close to 1 nm. In fact, detailed image analysis gave a center-to-center distance of 0.958 nm.

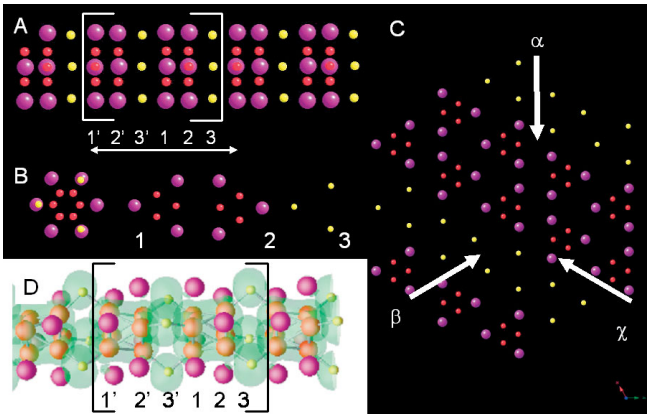

Figure 2. A) The structure of a $Mo_6S_3I_6$ nanowire as determined by Meden et al. [6]. Red, purple, and yellow spheres represent Mo atoms, and P and L sites, respectively. Having determined the nanowire structure using STEM, we can assign I atoms to the P sites (purple) and S atoms to the L sites (yellow). The brackets define the nanowire unit cell, which contains 12 Mo, 6 S, and 12 I atoms. The unit-cell length (as illustrated by the arrow) is 1.197 nm, whereas the wire center-to-center distance is 0.958 nm. The various atomic planes that make up the unit cell are labeled with numbers. Planes 1 and 2 are mixed planes, whereas plane 3 is a linkage (L) plane. Planes 1′, 2′, and 3′ are identical to planes 1, 2, and 3 rotated by 180° around the long axis of the wire. B) The view along the long axis of the wire. Planes 1, 2, and 3 are shown individually from this direction. C) A representation of the bundle structure after transformation into the $P\bar{1}$ structure. This figure shows a cross section of a bundle, one atomic plane thick, as viewed along the bundle *c*-axis. The three high-symmetry directions are labeled by α, β, and χ. D) A real-space representation of the local density of states (DOS) at the Fermi energy (E_F). These states are formed by Mo 4d and S 3p orbitals, and are clearly delocalized along the tube.

ADF STEM images were recorded from 157 different straight regions of bundles that were lying on the support film. Of these 157 images, 46 consistently showed three different forms of lattice image, with bands of high intensity running parallel to the bundle axis. Representative examples of each of these three lattice image types are shown in Figure 3B–D. Of the total of 46 images recorded, images similar to those shown in Figures 3B–D were observed 13, 21, and 12 times, respectively. We associate these with the three high-symmetry directions where the individual wires project with a maximum distance between each layer of wires (see Fig. 2C). The strong parallel bands of intensity in these microscopy images are therefore projection images of rows of wires that lie in a plane parallel to the long axis of the wire and parallel to the viewing direction. Both the $P6_3$ and $R\bar{3}$ spacegroups have rotational-symmetry axes along the wire axis such that the three high-symmetry viewing directions should show identical images. The fact that three different image types were observed (Fig. 3B–D) immediately suggests deviations from the previously predicted structure.

Looking at Figure 3B in more detail, we can see a strong zigzag pattern within a row that repeats every 0.4 nm. Of the

 © 2007 WILEY-VCH Verlag GmbH & Co. KGaA, Weinheim

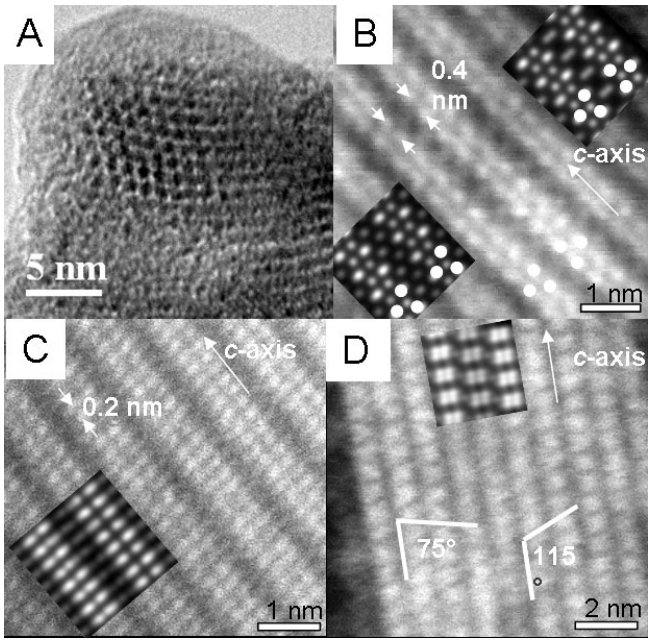

Figure 3. A) A TEM image of a bundle that is aligned with its *c*-axis parallel to the viewing direction. The close packing of the wires to form a bundle can be seen. B–D) Experimental ADF STEM images and (inset) image simulations of bundles viewed along the high-symmetry directions shown as α (B), β (C), and χ (D). All the image simulations used the proposed $P\bar{1}$ structure except the lower-left one in (B), which is of the $R\bar{3}$ structure.

proposed space groups, only $R\bar{3}$ gives a projection in which this zigzag pattern can be observed. However, simulation of images for the $R\bar{3}$ structure predicts that the zigzag pattern should be aligned such that the zigzag is in phase between neighboring rows (Fig. 3B, lower-left inset): the experimental image in Figure 3B shows that the zigzag is antiphase between neighboring rows. In more than 150 microscopy images, the in-phase alignment was never observed, further suggesting that neither $P6_3$ or $R\bar{3}$ correctly predict the structure.

A simple modification to the $R\bar{3}$ structure results in a bundle structure whose projected image more closely matches Figure 3B. One row of nanowires along one of the high-symmetry directions is chosen as the origin. The adjacent row on one side is shifted by one interlayer spacing, the next row by two spacings, and so on. Similarly, rows on the opposite side would be shifted in the opposite direction. This forces the zigzag patterns to have the correct alignment. Obviously, the proposed transformation breaks the threefold rotational symmetry of the trigonal $R\bar{3}$ spacegroup, and we can now expect the three high-symmetry viewing directions to show different patterns. This is shown in Figure 2C, which depicts a single atomic plane of a bundle after transformation, viewed along the long axis of the bundle. Along the direction labeled as χ, the L planes now project cleanly. The experimental image for this direction (Fig. 3D) shows that the intensity falls to close to background levels right across the L plane. This can only be explained if only the very weakly scattering S atoms lie in the L planes (L sites). The presence of I would give stronger scattered intensity (see Supporting Information and Fig. S2) meaning that the I atoms must lie in the P sites in the mixed planes. Thus, Figure 2 represents the actual wire structure with the red, purple, and yellow spheres depicting Mo, I, and S atoms, respectively.

Using this allocation of the I and S atoms, insets in Figure 3B–D show image simulations for a nanowire bundle from the three high-symmetry directions, α, β, and χ (shown in Figure 2C), for our new shifted structure. These now show an excellent match with the corresponding experimental images. In addition, this structure can explain every image we have measured. We now conclude that the wires do indeed contain individual strands consisting of mixed and L planes, as shown in Figure 2A and B. These strands then close-pack, but the shifts of layers preclude any rotational symmetry, resulting in a triclinic lattice. A center of symmetry allows the spacegroup to be identified as $P\bar{1}$ (#2), with the lattice parameters and atomic sites listed in the Supporting Information.

To confirm our structural assignment, XPS was carried out, as shown in the Supporting Information, Figure S3A–D. Deconvolution of the Mo 3d peak indicated that two Mo species were present. The main Mo component (blue) at binding energies (228.0 ± 0.1) eV and (231.9 ± 0.1) eV[19–21] is similar to that expected from MoS_x. This component comprises 87 % of the total Mo signal. An additional component (red) at (228.9 ± 0.1) eV and (231.9 ± 0.1) eV can be attributed to $(Mo_6I_8)I_4$ clusters[22,23] but only comprises 13 % of the Mo signal. Coupled with the TEM data, the observation that the majority of Mo atoms occupy identical sites supports the conclusion that the S atoms are all contained in the L planes (L sites), and that the mixed planes contain just Mo and I. The smaller peaks corresponding to $(Mo_6I_8)I_4$ clusters may be attributed to impurities similar to the well-known Chevrel phases.[17]

In addition, the S 2p signal is informative. This signal was deconvolved into a number of components (dotted) lines as shown in the Supporting Information, Figure S3C. The peak at (168.2 ± 0.1) eV can be attributed to residual impurities in the form of various oxidized sulfur compounds, as clearly shown by the comparison with the spectrum caused by impurities that had previously been removed from the sample[7] (Supporting Information, upper inset of Fig. S3C). The main lines at 160.9 eV and 162.3 eV are assigned as MoS_x species. The narrow line width of these S 2p signals shows that only one type of S bonding exists within the nanowire. As the STEM measurements rule out the possibility of the S atoms existing in the mixed planes, this confirms that they must all lie in the L plane. Coupled with the evidence that the I atoms are in mixed-plane sites, this confirms our assignment of the nanowire unit cell.

The average stoichiometry of the nanowires can also be confirmed by using XPS. Consideration of all the nanowire atomic contributions gives $Mo_{29}S_{15}I_{36}$. This is extremely close to the predicted stoichiometry of $Mo_6S_3I_6$ (compare with $Mo_{30}S_{15}I_{30}$). This small iodine excess (corresponding to

© 2007 WILEY-VCH Verlag GmbH & Co. KGaA, Weinheim

ADVANCED MATERIALS

ca. 1 I_2 per unit cell) is almost certainly caused by the residual iodine remaining from the synthesis.

The electronic properties of the wire were investigated using density functional theory (DFT).[24] The band structure along the tube axis and the corresponding density of states (DOS) for isolated $Mo_6S_3I_6$ are presented in Figure 4A and B. These demonstrate the metallic nature of the wires: a 0.8 eV wide band crosses the Fermi level (E_F). Its orbital charac-

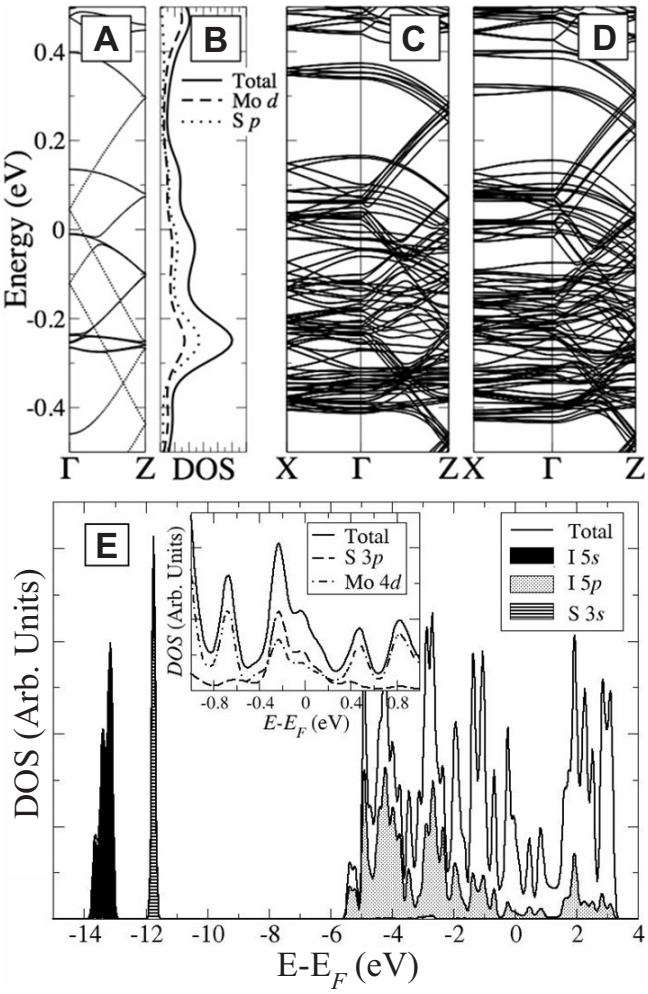

Figure 4. The electronic structure of MoSI wires and bundles. A) The bandstructure of an isolated $Mo_6S_3I_6$ wire along the wire axis, and corresponding B) orbital-resolved DOS. Bandstructure for C) $R\bar{3}$ and D) $P\bar{1}$ bundles in the directions across the bundle (X-to-Γ) and along the bundle axis (Γ-to-Z). E) Orbital-resolved DOS for an isolated wire over the entire valence energy range.

ter is dominated by Mo 4d and S 3p states, as confirmed by the local DOS (Fig. 2D), which demonstrates that it is delocalized along the tube. Such a band can support metal-like conductivity, although its narrowness suggests sensitivity to disorder and interwire interaction.

Mo–S hybridization forms the main chemical bond of the wire, and these orbitals dominate the DOS for about 10 eV around E_F (Fig. 4E). From Mulliken analysis we deduce a charge transfer of about 0.4 electrons from Mo 4d to S 3p per S atom. This gives us an oxidation state for Mo between Mo^{3+} and Mo^{2+}, in agreement with XPS results. In contrast, I retains a nearly atomic configuration. Interestingly the occupied I 5p states are rather broad, suggesting some level of interaction with the Mo ions.

The band structures of both the $R\bar{3}$ (Fig. 4C) and $P\bar{1}$ (Fig. 4D) bundles are rather similar to each other, and indeed to those of isolated wires. Both the bands in the direction across the bundle (X-to-Γ) are extremely flat, indicating a lack of interwire interaction. Along the tube axis (Γ-to-Z), they resemble those of isolated nanowires, with the addition of a small amount of band splitting, particularly in the case of the low-symmetry $P\bar{1}$ structure. Finally, as the total energy difference between the two structures is less than 0.2 meV per atom, DFT cannot determine the relative stability of these structures.

The lack of strong bonding between neighboring strands predicted by the DFT suggests that the interwire interaction can be attributed to weak dispersion/London interactions. To estimate the London interaction between wires for both the $R\bar{3}$ structure, and our proposed $P\bar{1}$ structure, we summed an energy term using the London equation[25] for every pair of atoms within a bundle consisting of 37 strands and with length of 3.6 nm (3 unit cells) in the c direction. The $P\bar{1}$ structure was found to be 18 eV lower in energy than $R\bar{3}$, suggesting that the interwire London interaction between the P atoms is optimized through the layer shifts that result in our proposed $P\bar{1}$ structure. The lowering in energy corresponds to approximately 170 meV $wire^{-1}$ nm^{-1}. A similar calculation results in a bundle cohesive energy of 3.0 eV $wire^{-1}$ nm^{-1}. This value is comparable to the cohesive energy of bundles of C nanotubes calculated by Girifalco et al. (ca. 2.4 eV $tube^{-1}$ nm^{-1}).[26] However, we note that $Mo_6S_3I_6$ nanowires are more readily dispersed in solvents relative to carbon nanotubes, despite their higher cohesive energy.

In conclusion, nanomaterials such as $Mo_6S_3I_6$ often appear in disordered form. Even advanced techniques such as the XAFS and PDF methods have not been able to determine the detailed structure. This is a huge problem as functional properties crucially depend on subtle structural details. The present combination of atomic-resolution aberration-corrected STEM, XPS, and modeling allows us to takes a great leap forward in structural determination. These techniques show that $Mo_6S_3I_6$ forms into nanowires consisting of a series array of well-defined unit cells. These wires then self-assemble into crystalline bundles. The nanowire unit cell consists of six stacked atomic planes: four mixed planes containing both Mo and I and two L planes containing S. The nanowires pack in crystalline bundles defined by the $P\bar{1}$ (#2) spacegroup.

DFT calculations demonstrate the metallic nature of these nanostructures, in which the Mo d–S p hybridization is responsible for the wire stability. We can further show that the self-assembly of the wires into the $P\bar{1}$ structure is driven by the minimization of London interaction energy. This allows the calculation of the bundle cohesive energy of ca. 3.0 eV $wire^{-1}$ nm^{-1}. It is most surprising and interesting that such a high degree of order is present in the bundles in

 © 2007 WILEY-VCH Verlag GmbH & Co. KGaA, Weinheim

spite of the relatively low cohesive energy. The modifications of the electronic structure of isolated wires when assembled in a bundle are tiny, however, because the conducting bands at the Fermi level are narrow and soft-bundle phonon modes are probably present, these wires are unlikely to behave as ballistic conductors. Still, they have a huge potential for nano-interconnects, as the presence of S in the linkage sites is ideal for linking to gold-terminated external connections.

Experimental

Molybdenum sulfur iodine nanowire material was synthesized in a single-step reaction directly from the elements in a sealed ampoule as described previously [4]. SEM images of this material were taken using a JEOL JXA-840A. The as-produced material was first washed repeatedly with acetone to remove excess molecular iodine. The washed material was then purified using controlled sedimentation as described by Nicolosi et al. [8]. Dispersions were prepared by sonication of the purified material in isopropyl alcohol at a concentration of 0.1 $mg\,mL^{-1}$. This resulted in dispersions consisting of bundles with diameters ranging from 1 to 40 nm. Samples for HRTEM and STEM were prepared by drop-casting onto holey Carbon grids (mesh size 400). HRTEM was performed using a JEOL-3000F and STEM was performed using a VG HB501 100 kV instrument and a VG Microscopes HB603U 300 kV instrument, both fitted with a Nion Cs corrector. Samples for XPS were prepared by deposition on silicon substrates. XPS measurements were carried out on a Kratos Axis HS and Mg Kα X-ray source.

Simulations of the aberration-corrected STEM images were computed following the simple method previously described by Cosgriff and Nellist [27]. Because the nanowire bundles are narrow, and strong channeling conditions were not established, the simulation method was as follows: First the electrostatic scattering potential was projected to form a 2D function. This projected potential function was then raised to the power of 1.7. Note that pure Rutherford scattering would result in a square dependence, but screening effects reduce this somewhat. The scaled projected potential was then convolved with the probe intensity function for the imaging conditions used as the image was recorded.

Samples for XPS measurements were produced by depositing an isopropyl alcohol suspension of the nanowires on precleaned silicon substrates and was left in air to dry, followed by immediate insertion into an ultrahigh vacuum (UHV) chamber. All the spectra were taken in normal emission geometry using Mg Kα radiation (photon energy 1253.6 eV). An overall energy resolution of 0.9 eV was determined from the Gaussian line width of the Au 4f of the clean gold foil. All the measurements were carried out in 10^{-9} torr (1 torr = 133.322 Pa) range using a 127 mm hemispherical analyzer.

All the peak positions were obtained by fitting the peaks with Gaussian–Lorentzian line shapes. The Gaussian component accounts for the instrumental energy resolution and the Lorentzian width accounts for the finite core-hole lifetime associated with the photoionization process. The background of the photoelectron intensity was subtracted by the Shirley background [28]. Binding energies in the core level spectra were calibrated by taking the binding energy of the Silicon $2p_{3/2}$ main line as 99.7 eV.

DFT calculations were performed with the code Siesta [24]. The generalized gradient approximation (GGA), as parameterized in Perdew et al. [29], was used for the exchange correlation potential. This systematically improved the description of the structural and electronic properties of molecules with respect to the local density approximation. For more details see the Supporting Information.

Received: August 15, 2006
Revised: November 9, 2006
Published online: January 24, 2007

[1] R. Sordan, K. Balasubramanian, M. Burghard, K. Kern, *Appl. Phys. Lett.* **2006**, *88*, 053 119.
[2] G. K. Mor, O. K. Varghese, M. Paulose, C. A. Grimes, *Sens. Lett.* **2003**, *1*, 42.
[3] M. Remskar, A. Mrzel, Z. Skraba, A. Jesih, M. Ceh, J. Demsar, P. Stadelmann, F. Levy, D. Mihailovic, *Science* **2001**, *292*, 479.
[4] D. Vrbanic, M. Remskar, A. Jesih, A. Mrzel, P. Umek, M. Ponikvar, B. Jancar, A. Meden, B. Novosel, S. Pejovnik, P. Venturini, J. C. Coleman, D. Mihailovic, *Nanotechnology* **2004**, *15*, 635.
[5] R. Murphy, V. Nicolosi, Y. Hernandez, D. McCarthy, D. Rickard, D. Vrbanic, A. Mrzel, D. Mihailovic, W. J. Blau, J. N. Coleman, *Scr. Mater.* **2006**, *54*, 417.
[6] A. Meden, A. Kodre, J. P. Gomilsek, I. Arcon, I. Vilfan, D. Vrbanic, A. Mrzel, D. Mihailovic, *Nanotechnology* **2005**, *16*, 1578.
[7] V. Nicolosi, D. Vrbanic, A. Mrzel, J. McCauley, S. O'Flaherty, C. McGuinness, G. Compagnini, D. Mihailovic, W. J. Blau, J. N. Coleman, *J. Phys. Chem. B* **2005**, *109*, 7124.
[8] V. Nicolosi, D. Vrbanic, A. Mrzel, J. McCauley, S. O'Flaherty, D. Mihailovic, W. J. Blau, J. N. Coleman, *Chem. Phys. Lett.* **2005**, *401*, 13.
[9] V. Nicolosi, D. Vengust, D. Mihailovic, W. J. Blau, J. N. Coleman, *Chem. Phys. Lett.* **2006**, *425*, 89.
[10] M. Zumer, V. Nemanic, B. Zajec, M. Remskar, M. Ploscaru, D. Vengust, A. Mrzel, D. Mihailovic, *Nanotechnology* **2005**, *16*, 1619.
[11] L. Joly-Pottuz, F. Dassenoy, J. M. Martin, D. Vrbanic, A. Mrzel, D. Mihailovic, W. Vogel, G. Montagnac, *Tribol. Lett.* **2005**, *18*, 385.
[12] G. Paglia, E. S. Bozin, D. Vengust, D. Mihailovic, S. J. L. Billinge, *Chem. Mater.* **2006**, *18*, 100.
[13] M. Haider, S. Uhlemann, E. Schwan, H. Rose, B. Kabius, K. Urban, *Nature* **1998**, *392*, 768.
[14] P. D. Nellist, M. F. Chisholm, N. Dellby, O. L. Krivanek, M. F. Murfitt, Z. Szilagyi, A. R. Lupini, A. Borisevich, W. H. J. Sides, S. J. Pennycook, *Science* **2004**, *305*, 1741.
[15] U. Falke, A. L. Bleloch, M. Falke, S. Teichert, *Phys. Rev. Lett.* **2004**, *92*, 116 103.
[16] P. D. Nellist, S. J. Pennycook, *Adv. Imag. Electron Phys.* **2000**, *113*, 148.
[17] T. Hughbanks, R. Hoffmann, *J. Am. Chem. Soc.* **1983**, *105*, 1150.
[18] R. Knoll, S. D. Goren, C. Korn, A. Shames, C. Perrin, A. Privalov, H. M. Vieth, *Phys. Rev. B: Condens. Matter* **2002**, *324*, 157.
[19] D. Briggs, M. P. Seah, *Practical Surface Analysis*, Wiley, New York **1993**.
[20] A. Galtayries, J. Grimblot, J. Wisniewski, *J. Electron Spectrosc. Relat. Phenom.* **1997**, *87*, 31.
[21] C. D. Wagner, J. F. Moulder, L. E. Davis, W. M. Riggs, *Handbook of X-ray Photoelectron Spectroscopy*, 1st Ed., Perkin–Elmer, Eden Prairie, MN **1979**.
[22] S. A. Best, R. A. Walton, *Inorg. Chem.* **1979**, *18*, 484.
[23] K. Kirakci, S. Cordier, C. Perrin, *Z. Anorg. Allg. Chem.* **2005**, *631*, 411.
[24] J. M. Soler, E. Artacho, J. D. Gale, A. Garcia, J. Junquera, P. Ordejon, D. Sanchez-Portal, *J. Phys. Condens. Matter* **2002**, *14*, 2745.
[25] P. W. Atkins, R. S. Friedman, *Molecular Quantum Mechanics*, Oxford University Press, Oxford **1997**.
[26] L. A. Girifalco, M. Hodak, R. S. Lee, *Phys. Rev. B: Condens. Matter* **2000**, *62*, 13 104.
[27] E. C. Cosgriff, V. Nicolosi, J. N. Coleman, P. D. Nellist, in *Proc. of EMAG-NANO 05*, IOP Publishing, Bristol, UK **2006** p. 280.
[28] D. A. Shirley, *Phys. Rev. B: Solid State* **1972**, *5*, 4709.
[29] J. P. Perdew, K. Burke, M. Ernzerhof, *Phys. Rev. Lett.* **1996**, *77*, 3865.

© 2007 WILEY-VCH Verlag GmbH & Co. KGaA, Weinheim